Acta Cryst. (1988). A**44**, 128-135

Short-Range-Order Correlations in the Orientationally Disordered Phase of Hexachloroethane. I. Diffuse X-ray Scattering

BY P. GERLACH* AND W. PRANDL

Institut für Kristallographie der Universität Tübingen, Charlottenstrasse 33, D-7400 Tübingen, Federal Republic of Germany

(*Received* 15 *September* 1986; *accepted* 17 *September* 1987)

Abstract

Diffuse X-ray scattering has been measured in the orientationally disordered phase of C_2Cl_6 at 453 K. A model structure, which was generated in a Monte Carlo program, reproduces the dominant single-molecule part of the diffuse scattering. In addition the existence of a one-dimensional orientational order along the body diagonals of the cubic lattice is demonstrated. The related planes of diffuse scattering are calculated in terms of the Naya model [Naya (1974). *J. Phys. Soc. Jpn*, **37**, 340-347].

1. Introduction

Rotational excitations in molecular crystals are in most cases described as single-particle rotations (Press, 1981). The complex picture of the rotational degrees of freedom is in this approximation restricted to the description of the motion of a single molecule in its surroundings. There are two principal reasons why this approximation is widely used: (i) in cases where the intermolecular interactions are relatively weak, the description of the molecular motion occurring without phase relationship with its neighbours seems intuitively to be a good approximation, and (ii) incoherent neutron scattering provides an experimental probe which can observe single-particle motions directly (Bee, 1985). In order, however, to detect collective phenomena, which play an essential role in the understanding of structural phase transitions, one has to analyse the coherent diffuse scattering.

This paper is the first part of a report about a combined X-ray and neutron scattering study of the coherent diffuse scattering in the orientationally disordered phase of hexachloroethane. The analysis of the X-ray data gives a static description of the disorder, while in the second part elastic and quasielastic neutron scattering will reveal dynamic aspects of the disorder.

From a symmetry point of view, one can distinguish two different types of orientationally disordered molecular crystals: the molecular symmetry is (i) lower than or (ii) equal to the lattice site symmetry. In the first case a number of symmetry-related equilibrium orientations are necessary to satisfy the site symmetry. The disorder in the latter case is given by large-amplitude librational and translational motions around the single equilibrium orientation. Hexachloroethane falls between these two categories. It crystallizes between 344·1 K and the melting point at 458 K in a cubic body-centred structure with space group $Im3m$ ($a = 7{\cdot}50$ Å, $Z = 2$). The molecular symmetry is $\bar{3}m$ and therefore lower than the cubic site symmetry $m3m$, but the distortion from a regular octahedron, which would have the full cubic symmetry, is small. Two phase transitions have been observed at 316·6 and 344·1 K. The low-temperature phase is ordered and has the orthorhombic space group *Pnma* (Hohlwein, Nägele & Prandl, 1979), while the intermediate phase is monoclinic with a still unknown space group.

The outline of the present paper is as follows. A brief summary of the relations needed to describe the X-ray and energy-integrated coherent neutron scattering is contained in § 2. The experimental results are given in § 3. In order to establish the existence and nature of correlations the data are first analysed in terms of various single-molecule models (§ 4). As part of this a model structure is generated in a Monte Carlo program which takes into account the hard-core interactions between neighbouring molecules. This simulation method has been used previously in the analysis of the neutron Bragg scattering data (Gerlach, Prandl & Lefebvre, 1983). The advantage of this analysis is its universality, which allows us to include continuous scattering density functions, translational-orientational correlation effects and non-harmonic types of motion. Semi-empirical atom-atom potentials are used in § 5 to describe the short-range interaction between the non-polar C_2Cl_6 molecules so that the orientational correlations in the Naya model can be determined (Naya, 1974). The results are summarized in § 6 where a consistent picture of the disorder is formulated. This view will be used as the basis for the inelastic neutron study to be described in paper II.

* Present address: Physikalisches Institut der Universität Kiel, Olshausenstrasse 40, D-2300 Kiel 1, Federal Republic of Germany.

0108-7673/88/020128-08$03.00

2. Theory

In a plastic crystal, reorientational jumps and large-amplitude translational and librational motions cause fluctuations in both the centre-of-mass position and the orientation of a molecule (internal degrees of freedom are neglected throughout this paper). In analogy with the Ising model we use a vector $\boldsymbol{\mu}_j$ to specify a particular state of the molecule at the lattice site j. The dimension of $\boldsymbol{\mu}$ is given by the total number s of discrete states which the molecule is able to occupy. Each component μ_j^l can take the value 1 or 0, depending on whether the state l is occupied or not. In general each state is characterized by a certain orientation $\boldsymbol{\Omega}$ and a centre-of-mass deviation vector $\mathbf{u}$.

The energy-integrated coherent scattering can be written in the form

$$I(\mathbf{Q}) = \mathbf{f}\langle\boldsymbol{\mu}(\mathbf{q}) \cdot \boldsymbol{\mu}(\mathbf{q})\rangle\mathbf{f}^* \tag{1}$$

where $\langle\boldsymbol{\mu}(\mathbf{q}) \cdot \boldsymbol{\mu}(\mathbf{q})\rangle$ is the Fourier-transformed thermal fluctuation function

$$\langle\boldsymbol{\mu}(\mathbf{q}) \cdot \boldsymbol{\mu}(\mathbf{q})\rangle = \sum_i \sum_j \langle\boldsymbol{\mu}_i \cdot \boldsymbol{\mu}_j\rangle \exp(i\mathbf{q}\mathbf{R}_{ij}). \tag{2}$$

The summation goes over all lattice points i and j which are separated by the vector $\mathbf{R}_{ij}$. The component l of the s-dimensional vector f is the molecular form factor of state l,

$$f^l(\boldsymbol{\Omega}, \mathbf{u}) = \sum_{i=1}^{N_{at}} a_i(Q) \exp[-i\mathbf{Q}\mathbf{r}_i^l(\boldsymbol{\Omega}, \mathbf{u})],$$

where $\mathbf{r}_i^l$ is the position vector of each of the N_{at} atoms of the molecule. The atomic scattering factor $a_i(Q)$ for X-rays has to be replaced in the neutron case by the Q-independent coherent scattering length b_i.

In order to separate the Bragg scattering I_B from the diffuse scattering (I_{D1} and I_{DC}), which is the subject of the present paper, we rearrange (1) to read

$$I(\mathbf{Q}) = I_B + I_{D1} + I_{DC} \tag{3}$$

with

$$I_B = \langle f(\mathbf{Q})\rangle^2 \sum_{i,j} \exp(i\mathbf{q}\mathbf{R}_{ij}) \tag{4}$$

$$I_{D1} = \langle f(\mathbf{Q})^2\rangle - \langle f(\mathbf{Q})\rangle^2 \tag{5}$$

$$I_{DC} = \sum_{i,j} \langle f_i f_j\rangle \exp(i\mathbf{q}\mathbf{R}_{ij}) \quad i \neq j. \tag{6}$$

The angular brackets denote thermal averages, which are defined by

$$\langle f\rangle = \mathbf{f}\langle\boldsymbol{\mu}\rangle \tag{7}$$

$$\langle f^2\rangle = \mathbf{f}(\langle\boldsymbol{\mu} \cdot \boldsymbol{\mu}\rangle)\mathbf{f}^* \tag{8}$$

$$\langle f_i f_j\rangle = \mathbf{f}(\langle\boldsymbol{\mu}_i \cdot \boldsymbol{\mu}_j\rangle - \langle\boldsymbol{\mu} \cdot \boldsymbol{\mu}\rangle)\mathbf{f}^*. \tag{9}$$

In a phenomenological statistical description of the disorder, the correlation function $\langle\boldsymbol{\mu}_i \cdot \boldsymbol{\mu}_j\rangle$ in direct space represents a joint probability (Matsubara, 1950). The probability of finding the molecule i at the lattice point i in state l is given by the component $\langle\mu_i^l\rangle$. $\langle\mu_i^l \cdot \mu_j^m\rangle$ is the joint probability that the molecule i is in the molecular state denoted by l and that at the same time the molecule j is in state m. Correlation effects [equation (9)] are then specified by the difference of the joint probability and the uncorrelated distribution $\langle\boldsymbol{\mu} \cdot \boldsymbol{\mu}\rangle$.

The Bragg scattering I_B [equation (4)] is the scattering by the time-averaged mean crystal structure, while the diffuse scattering reflects deviations from the mean. I_{D1} is the single-molecule scattering, which is the total diffuse scattering in the limit of vanishing correlations. In the presence of correlations I_{D1} will be modulated by the term I_{DC}.

$$I_D = I_{D1} + I_{DC} = \mathbf{f}(\mathbf{Q})(\langle\boldsymbol{\mu}_q \cdot \boldsymbol{\mu}_q\rangle - \langle\boldsymbol{\mu}_q\rangle\langle\boldsymbol{\mu}_q\rangle)\mathbf{f}^*(\mathbf{Q}). \tag{10}$$

The different symbols $\mathbf{q}$ and $\mathbf{Q}$ were chosen in order to distinguish between Fourier transforms of distances in the lattice and molecule, respectively. For example, $\boldsymbol{\mu}(\mathbf{q})$ shows the periodicity of the reciprocal lattice and therefore it holds that

$$\boldsymbol{\mu}(\mathbf{Q}) = \boldsymbol{\mu}(\mathbf{q})$$

with

$$\mathbf{Q} = 2\pi\boldsymbol{\tau} + \mathbf{q}$$

where $\boldsymbol{\tau}$ is a reciprocal-lattice vector and $\mathbf{q}$ is a vector pointing from the origin to a point inside the Brillouin zone.

The aim of a microscopic description of the disordered structure is to explain the thermal fluctuations of (2) as a result of the molecular interactions. A most elegant way to do so is to introduce a wave-vector-dependent generalized susceptibility $\chi(\mathbf{q})$ (Kubo, 1957; Descamps & Coulon, 1981; Nagai, 1982) which allows one to obtain the Fourier components of the microscopic fluctuations $\langle\boldsymbol{\mu}_q\rangle$ in response to local static perturbations $\mathbf{h}_q$ conjugate to $\boldsymbol{\mu}_q$,

$$\chi(\mathbf{q}) = \partial\langle\boldsymbol{\mu}_q\rangle/\partial\mathbf{h}_q = \beta(\langle\boldsymbol{\mu}_q\boldsymbol{\mu}_q\rangle - \langle\boldsymbol{\mu}_q\rangle\langle\boldsymbol{\mu}_q\rangle). \tag{11}$$

In the following we consider only correlations between different orientational molecular states, which are described by the vector $\boldsymbol{\mu}^R$. The Hamiltonian for the total system can then be expressed as a sum over pair interaction energies between all molecules on different lattice sites and an additional interaction with the perturbation field. In the molecular-field (random-phase) approximation the first interaction, depending on the configurations, is replaced by an averaged field acting at the site of the molecule considered. The interaction Hamiltonian is in $\mathbf{q}$ space

$$H = \boldsymbol{\mu}_q^R \mathbf{J}_q \langle\boldsymbol{\mu}_q^R\rangle + \mathbf{h}_q \boldsymbol{\mu}_q^R \tag{12}$$

where $\mathbf{J}_q$ is the Fourier-transformed interaction-energy matrix.

Together with the definition for the mean value

$$\langle \boldsymbol{\mu}_q^R \rangle = \sum_{\mu_q} \boldsymbol{\mu}_q^R \exp(-\beta H) / \sum_{\mu_q} \exp(-\beta H) \quad \beta = 1/kT, \tag{13}$$

$\langle \boldsymbol{\mu}_q^R \rangle$ can be determined self-consistently. Substitution of (13) into (11) gives the generalized susceptibility in terms of the interaction energy (Naya, 1974):

$$\partial \langle \boldsymbol{\mu}_q^R \rangle / \partial \mathbf{h}_q = \beta \mathbf{M}[\mathbf{1} + \beta \mathbf{J}(\mathbf{q})\mathbf{M}]^{-1}. \tag{14}$$

Here β is the inverse temperature $1/kT$ and $\mathbf{M}$ is a q-independent momentum matrix whose elements depend on the total number of discrete states s,

$$M^{kl} = 1/s\delta_{kl} - 1/s^2.$$

Equation (14) shows that fluctuations in the orientational molecular states from their thermal average reflect directly the $\mathbf{q}$ or, in direct space, the $\mathbf{r}$ dependence of the microscopic interaction $\mathbf{J}(\mathbf{r})$. These fluctuations are experimentally observable in the diffuse X-ray and coherent neutron scattering as stated in (1). The Bragg scattering expressed in (4), on the other hand, is proportional to the mean value of $\langle \boldsymbol{\mu} \rangle$ and can be used to determine in an analogous way an effective (rotational) potential acting on an individual molecule (Gerlach, Prandl & Vogt, 1984).

The orientational fluctuations derived in (14) diverge for wave vector q_0 and temperature T_c at which

$$|\mathbf{1} + (1/kT_c)\mathbf{M}\mathbf{J}(\mathbf{q}_0)| = 0. \tag{15}$$

T_c is therefore the first-order phase-transition temperature to an orientationally ordered phase.

3. Experimental

Single crystals of hexachloroethane in the plastic phase were grown by slow cooling from the melt. Since C_2Cl_6 sublimes in air, the melt and the crystal were always sealed in a thin-walled glass capillary. The background scattering from the capillary was negligible in comparison with the diffuse scattering from the sample. The crystals, with a volume of approximately 1 mm^3, had the cylindrical shape of the glass capillary and showed no preferred growth direction.

The diffuse X-ray scattering from C_2Cl_6 was recorded photographically by means of the monochromatic Laue technique. A schematic drawing of the recording geometry is shown in Fig. 1. In order to obtain a projection of a plane in reciprocal space with only a small distortion short-wavelength Mo radiation was used ($\lambda_{Mo\,K\alpha} = 0{\cdot}7117$ Å), which was monochromatized by a β filter. The flat photographic film was located 60 mm from the sample. The exposure time for typical photographs was 8 h. For a quantitative analysis the intensity distributions on the photographs were measured by a computer-controlled microdensitometer and converted into a linear densitogram. Photographs obtained at a temperature close to the melting point ($T = 453$ K) are shown in Fig. 2 for incidence parallel to high-

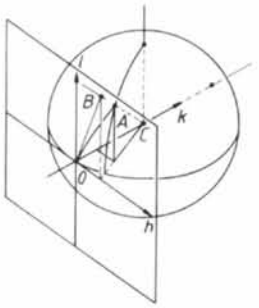

Fig. 1. Recording geometry for the monochromatic Laue technique with a flat film. The gnomonic projection relates the point B on the film with coordinates h^*0l^* to the point A in reciprocal space, which has coordinates hkl. The transformation is

$$h = h^*RA \quad k = R - R^2A \quad l = l^*RA$$

with $A = 1/(R^2 + h^{*2} + l^{*2})^{1/2}$ and R the radius of the Ewald sphere, $R = 1/\lambda a^*$. a^* is the length of the reciprocal basis vector of the cubic lattice.

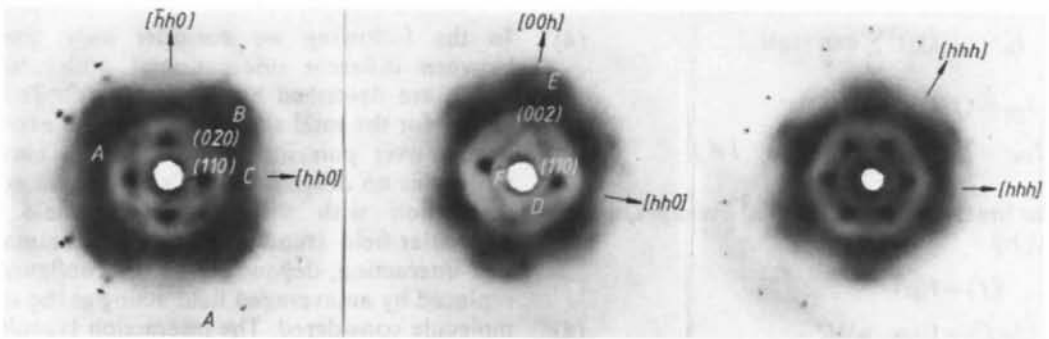

(a) (b) (c)

Fig. 2. Monochromatic Laue photographs of a single crystal of C_2Cl_6 in the plastic phase at $T = 453$ K taken with Mo $K\alpha$ radiation. The [100], [110] and [111] axis is along the direction of the incident beam in (*a*), (*b*) and (*c*), respectively. Features marked *A*, *B*, ..., are explained in the text.

symmetry directions. They all show a few Bragg reflections superimposed on a strong highly modulated diffuse background. The only Bragg spots observed by this method are those which coincide accidentally with the Ewald sphere in a certain symmetry direction. From (5) and (6) the diffuse scattering can be classified into two contributions: part of the diffuse scattering is distributed over extended areas and shows no pronounced modulation consistent with the underlying reciprocal lattice [equation (5)]. Characteristic features belonging to this contribution which are visible on all three photographs are two concentric halos (A in Fig. 2a), which have intensity maxima at $|\mathbf{Q}| = 2{\cdot}4$ and $3{\cdot}4$ Å^{-1}. These intensity maxima are in agreement with the diffuse intensity seen in a neutron powder experiment reported earlier (Gerlach, Hohlwein, Prandl & Schulz, 1981). While the outer halo is too weak to give any intensity modulation, the inner ring shows pronounced intensity maxima along the ⟨001⟩ (B) and ⟨011⟩ (C in Fig. 2a) directions. Only the latter can be attributed to spot-like diffuse scattering centred on the Bragg spot 220 (Fig. 3).

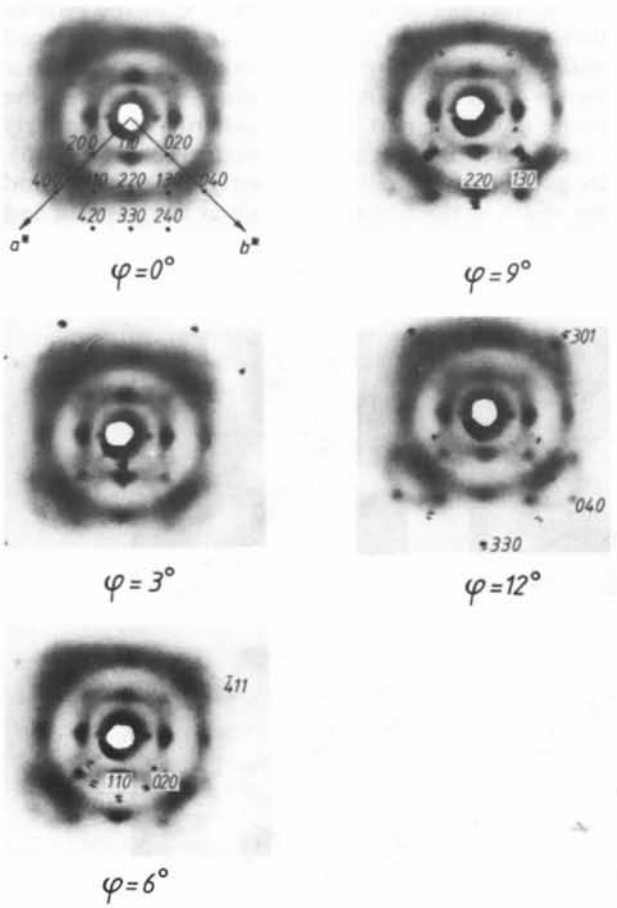

Fig. 3. A series of Laue photographs obtained by stepwise rotation of the crystal around the [$\bar{1}$10] axis by the angle ζ. Diffuse extensions of Bragg peaks are clearly separable from extended regions of diffuse intensity.

A second type of scattering is related to the reciprocal lattice. In order to demonstrate this, a series of photographs was obtained with step-by-step rotation of the crystal around one of the high-symmetry directions. Fig. 3 shows as an example a series of these low-symmetry projections. Characteristic features are:

Many Bragg spots are superimposed on a spot-like diffuse scattering, in particular the most intense 110 reflection.

Inside the first halo a diffuse streak system is observable. These streaks are clearly visible in regions where they form a connection between the 110 and 002 reflections (D in Fig. 2b), but seem to have also a more diffuse extension in the ⟨001⟩ direction around the forbidden lattice point 003 (E in Fig. 2b). A comparison of Figs. 2 and 3 demonstrates that these features are intersections of (111) planes of diffuse intensity with the Ewald sphere.

Relatively sharp 'superlattice reflections' appear at small scattering angles (F in Fig. 2b). On photographs taken with the precession technique - which show an undistorted section of the reciprocal space - their intensity maxima occur at $\mathbf{q} = 0{\cdot}6\mathbf{q}(110)$. No higher orders of these 'reflections' could be observed.

A preliminary investigation of the temperature dependence of these features showed no significant changes in the diffuse intensity distribution down to temperatures of about $T \simeq 1{\cdot}05\,T_c$. Unfortunately, it is not possible to cool the crystal into the monoclinic intermediate phase below $T_c = 344{\cdot}1$ K without destroying the monocrystal. However, more accurate measurements are planned using counter techniques to determine the temperature dependence of particular features of the diffuse intensity distribution.

4. The single-molecule scattering

Most of the observed diffuse intensity is distributed over large areas in reciprocal space and shows no modulation related to the underlying reciprocal space. This suggests a dominant contribution from single-molecule scattering. This scattering is proportional to the probability $\langle\boldsymbol{\mu}\rangle$. If we neglect correlation effects between the orientation and the centre-of-mass deviation of an individual molecule then we can write I_{D1} of (5) as (Dolling, Powell & Sears, 1979)

$$I_{D1} = I^R_{D1}(\boldsymbol{\Omega}) + I^T_{D1}(\boldsymbol{\Omega}, \mathbf{u}) \qquad (16)$$

where

$$I^R_{D1} = \langle f^2\rangle - \langle f\rangle^2 \quad \text{and} \quad I^T_{D1} = \langle f\rangle^2[1 - \exp(-2W)]$$
$$\langle f^2\rangle = \mathbf{f}\langle\boldsymbol{\mu}^R \cdot \boldsymbol{\mu}^R\rangle\mathbf{f} \quad \text{and} \quad \langle f\rangle = \mathbf{f}\langle\boldsymbol{\mu}^R\rangle. \qquad (17)$$

I^T_{D1} is the diffuse intensity caused by uncorrelated harmonic vibrations of the averaged molecule. The Debye–Waller factor $\exp(-2W)$ is the Fourier transformation of an isotropic centre-of-mass deviation

vector distribution. In contrast, I_{D1}^{R} is the contribution coming exclusively from the single-particle orientational disorder. Both terms calculated for a simple Frenkel model are shown in Fig. 4. The averaged molecule was obtained by applying the symmetry operations of the cubic site symmetry $m3m$ to a molecule with its trigonal axis pointing along one of the ⟨111⟩ crystal axes. The Debye–Waller factor was taken from the structure refinement [$\langle u^2\rangle = 0{\cdot}22$ Å^2 (Gerlach *et al.*, 1981)].

The diffuse scattering I_{D1}^{R} (Fig. 4*a*) is relatively weak and shows only maxima under large scattering angles, in disagreement with Fig. 2. This result reflects the relatively small distortion of the C_2Cl_6 molecule from a regular octahedron, making the different symmetry-related orientations in the Frenkel model almost indistinguishable. Even the very approximate description in terms of an isotropic Debye–Waller factor leads to an intensity distribution I_{D1}^{T} (Fig. 4*b*) which shows intensity maxima consistent with the experimental data in Fig. 2. This demonstrates clearly that the main cause of the disorder in the high-temperature phase of C_2Cl_6 is large-amplitude translational and librational motions rather than the statistical occupancy of different orientations.

A more realistic model structure of the plastic phase generated by a Monte Carlo method was described earlier and used for the interpretation of Bragg intensities (Gerlach, Prandl & Lefebvre, 1983). The averaged orientational–translational distribution for a single molecule was determined in this method by computing the sterically allowed configurations for the centre molecule in an 8 + 1 molecular cluster. This cluster represents the nearest-neighbour interactions in a body-centred cubic lattice. The model now removes three restrictive approximations considered above in the Frenkel model:

a sufficiently large number of allowed configurations approximates a quasi-continuous molecular scattering density distribution;

each allowed configuration is simultaneously a function of $\mathbf{u}$ and $\boldsymbol{\Omega}$; the model therefore takes into account translational–orientational correlations for a single molecule; and

the librational and translational motions are no longer treated harmonically.

The averaged structure factor $\langle f\rangle$ [equation (7)] is in this model given by a summation over N configurations,

$$\langle f(\mathbf{Q})\rangle = \sum_{n=1}^{N} P(S_n) f(S_n) \Big/ \sum_{n=1}^{N} P(S_n). \qquad (18)$$

$P(S_n)$ has the value 1 for a sterically allowed configuration and 0 otherwise. $\sum_{n=1}^{N} P(S_n)$ is the number of allowed configurations in a sample of size N.

The intensity distribution produced by the Fourier transformation of a model structure for the averaged molecule built up by 3000 allowed configurations is shown in Fig. 5. This calculation reproduces the single-molecule part of the scattering qualitatively much better than the simple Frenkel model (Fig. 4*b*). In particular, it predicts correctly the position and the width of the first ring as well as the position and form of the diffuse maxima located on this ring (*B* and *C* in Fig. 2). The intensity at larger scattering

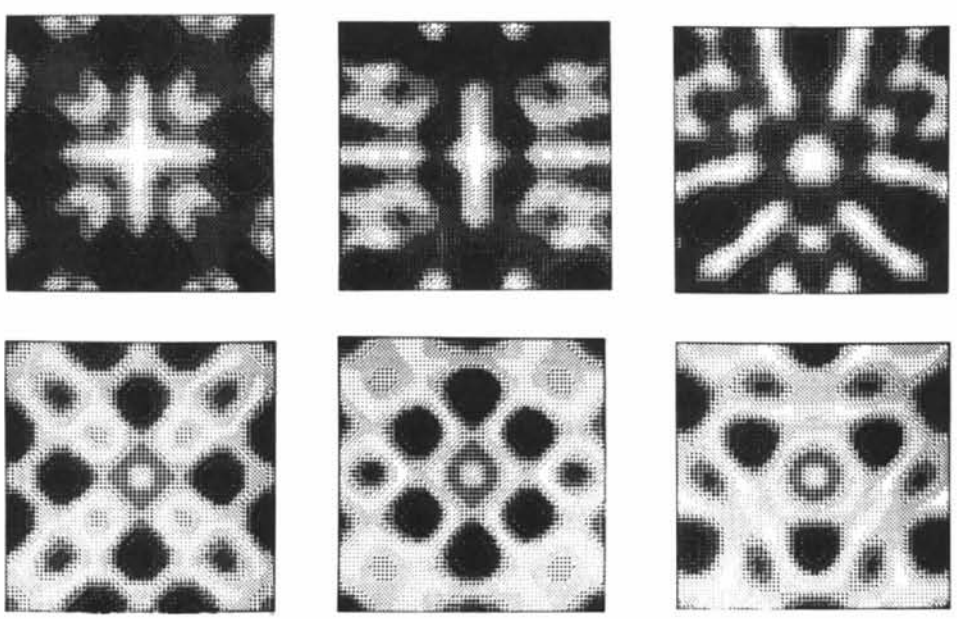

Fig. 4. The calculated single-molecule scattering for the Frenkel model. (*a*) The term I_{D1}^{R}; (*b*) I_{D1}^{T} [equation (17)]. The scattering planes correspond to Fig. 2. The intensity is shown on a linear scale with ten different grey tones between $I_{min} = 0$ and $I_{max} = 190$ and 2370 a.u. in (*a*) and (*b*) respectively.

angles, which was highly modulated in the Frenkel model, is now almost uniformly distributed on the halo in agreement with experiment. This analysis of the single-molecule scattering confirms in an illustrative way the conclusions drawn earlier from an analysis of the Bragg scattering (Gerlach, Hohlwein, Prandl & Schulz, 1981; Gerlach, Prandl & Lefebvre, 1983). The molecules perform large-amplitude librational motions around their equilibrium orientation. The trigonal molecular axes are distributed close to the cubic {111} axes with the Cl atoms near the {100} axes.

5. Diffuse scattering due to orientational correlations

The differences in the experimentally observed and calculated intensities with the single-molecule approximation indicate the existence of short-range-order correlations between different molecular states. The most obvious feature is the intensity localized in (111) planes in reciprocal space. This suggests in general a one-dimensional order in direct space perpendicular to these planes, *i.e.* along the cubic body diagonal (Guinier, 1963). Nearest neighbours lie along this direction in the body-centred cubic lattice.

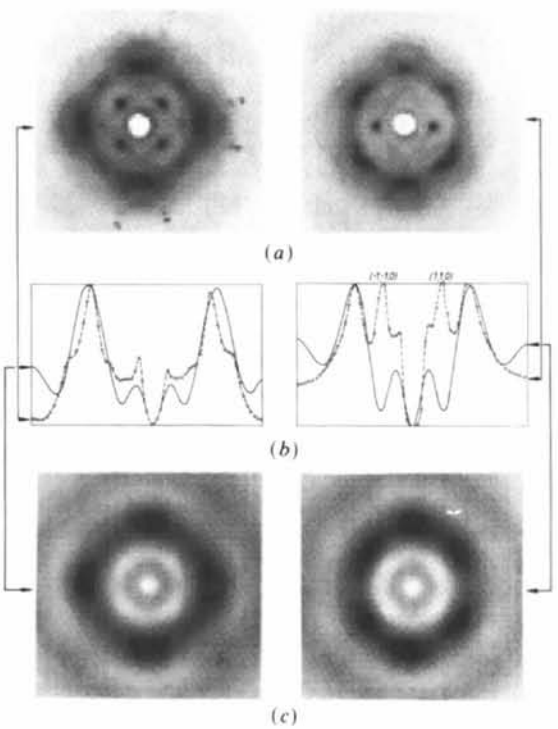

Fig. 5. Comparison between the observed (*a*) and calculated (*c*) single-molecule scattering using the Monte Carlo method. The linear densitogram uses 32 grey tones ($I_{min} = 0$, $I_{max} = 1280$ a.u.). (*b*) shows the calculated (——) and observed (- - -) intensity along the $[q, 0, 0]$ and $[q, q, 0]$ directions. Small differences in the calculated intensities at symmetry-related points are due to the limited number of molecules ($N = 3000$) used in the simulation routine.

Because the 8+1 molecule cluster which we used to determine the single-molecule scattering is too small to determine any correlation effects, we applied the analytical method described in § 2 to estimate the correlation scattering. We consider the hexachloroethane molecules lying with their trigonal axes parallel to the body diagonal of the cubic lattice. This leads to four distinguishable discrete orientations for each molecule, which are equally occupied. The interaction energies for the 16 possible nearest-neighbour configurations were calculated with the use of semi-empirical atom–atom potentials (Gerlach, Prandl & Vogt, 1984). The Fourier-transformed interaction matrices $\mathbf{J}_q$ [equation (12)], together with a schematic drawing of these configurations, are given in Table 1. For all centre-of-mass distances in the high-temperature phase ($\frac{1}{2}a\sqrt{3} = 6{\cdot}48$ Å at 335 K and 6·61 Å at 453 K) a parallel arrangement of the trigonal axes of neighbouring molecules is obviously energetically favourable. It should be emphasized at this point that the relatively small distortion of the actual molecular shape from a regular octahedron is the essential part of this disorder model, resulting in the energy differences shown in Table 1.

The transition temperature calculated by using this set of energies in (15) is unrealistically low (T_c = 11 K), but Fig. 6 demonstrates a strong dependence of the transition temperature on the interaction energies. An arbitrary change in the energy difference between the two lowest levels from 185 to 800 K increases the transition temperatures close to the observed value. The reason for this discrepancy between the calculated and observed transition temperatures is probably the restriction to only nearest-neighbour interactions. We shall use in the following the parameter set 3 in Fig. 6 for the computation of the diffuse intensity distribution. The momentum and structure-factor matrix are given in Table 2. An uncorrelated centre-of-mass motion is taken into account by the multiplication of the non-diagonal matrix elements in the structure-factor matrix with the Debye–Waller factor mentioned earlier. [The diagonal elements represent the intensity scattered by a single molecule, which is the first term in I_{D1} - see (5) - and therefore independent of the Debye–Waller factor.] Fig. 7 shows, for three different temperatures, typical intensity distributions in the scattering plane which corresponds to Fig. 2(*b*). The appearance of (111) planes of diffuse intensity which are most obvious in the (001) scattering plane (see Fig. 7*b*) is in agreement with experiment and proves the existence of short-range-order correlations along the cubic body diagonal. In contrast to an atomic crystal these two-dimensional intensities are only pronounced in regions where the molecular structure factor is strong, in the present case, for example, along the $[00q]$ direction for $q = 3{\cdot}0$ (*E* in Fig. 2).

Table 1. *The Fourier-transformed interaction energy matrices for* $a = 7{\cdot}63$ Å *at* 453 K (*EA, EB, ... refer to the* 16 *relative orientations between neighbouring molecules shown in the insert*)

$$\mathbf{J} = \sum_{k=1}^{4} \mathbf{J}_k[\exp(i\mathbf{q}\mathbf{R}_k) + \exp(-i\mathbf{q}\mathbf{R}_k)]$$

$$= 2\sum_{k=1}^{4} \mathbf{J}_k C_k$$

with

$$C_1 \equiv \cos \pi(h+k+l)$$
$$C_2 \equiv \cos \pi(-h+k+l)$$
$$C_3 \equiv \cos \pi(-h-k-l)$$
$$C_4 \equiv \cos \pi(h-k+l)$$

and

$$\mathbf{J}_1 = \begin{pmatrix} EA & EB & EB & EB \\ EB & EC & ED & ED \\ EB & ED & EC & ED \\ EB & ED & ED & EC \end{pmatrix} \qquad \mathbf{J}_2 = \begin{pmatrix} EC & EB & ED & ED \\ EB & EA & EB & EB \\ ED & EB & EC & ED \\ ED & EB & ED & EC \end{pmatrix}$$

$$\mathbf{J}_3 = \begin{pmatrix} EC & ED & EB & ED \\ ED & EC & EB & ED \\ EB & EB & EA & EB \\ ED & ED & EB & EC \end{pmatrix} \qquad \mathbf{J}_4 = \begin{pmatrix} EC & ED & ED & EB \\ ED & EC & ED & EB \\ ED & ED & EC & EB \\ EB & EB & EB & EA \end{pmatrix}$$

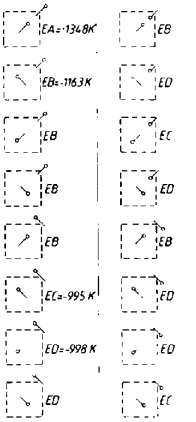

The calculation shows strong streaks connecting the origin in reciprocal space with the 110 reflections. No maxima are present along this direction at 0·6, 0·6, 0. This suggests that the diffuse spots observed at these points are caused by translational-translational or translational-orientational correlations which are omitted in these calculations.

With the increase in temperature the decaying orientational correlations produce a less-modulated pattern. For temperatures $T \gg T_c$ the correlation function (14) approaches unity and the intensity distribution becomes identical to the single-molecule scattering shown in Fig. 4(*b*). The limitation of the Naya model to only a small number of discrete orientations also produces here a diffuse scattering pattern, which is modulated too strongly in comparison with the experiment analogous to the Frenkel model.

Summary

We have interpreted the observed diffuse X-ray scattering in the plastic phase of C_2Cl_6 in terms of single-molecule scattering and by a theory which takes into account correlation effects in the orientational states of neighbouring molecules.

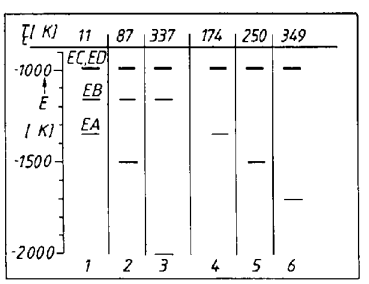

Fig. 6. The transition temperature [equation (15)] for different sets of interaction energies, which were defined in Table 1.

Table 2. *The momentum and structure-factor matrices*

$$\mathbf{M} = 1/16 \begin{pmatrix} 3 & -1 & -1 & -1 \\ -1 & 3 & -1 & -1 \\ -1 & -1 & 3 & -1 \\ -1 & -1 & -1 & 3 \end{pmatrix}$$

$$\mathbf{F} = \begin{pmatrix} f_1 f_1^* & f_1 f_2^* T & f_1 f_3^* T & f_1 f_4^* T \\ f_2 f_1^* T & f_2 f_2^* & f_2 f_3^* T & f_2 f_4^* T \\ f_3 f_1^* T & f_3 f_2^* T & f_3 f_3^* & f_3 f_4^* T \\ f_4 f_1^* T & f_4 f_2^* T & f_4 f_3^* T & f_4 f_4^* \end{pmatrix}$$

with the isotropic Debye-Waller factor

$$T = \exp[(-\langle \mathbf{u}^2 \rangle/2)Q^2]$$
$$Q = 4\pi^2(h^2+k^2+l^2)/a^2$$

and the molecular structure factors

$$f_i = 2f^{C}(Q)\cos[2\pi/a(hx_i^{C} + ky_i^{C} + lz_i^{C}]$$
$$+ \sum_{j=1}^{3} 2f^{Cl}(Q)\cos[2\pi/a(hx_{ij}^{Cl} + ky_{ij}^{Cl} + lz_{ij}^{Cl})].$$

The atomic coordinates for the four different orientations i are

			$i=1$	2	3	4
Carbon		x	d	$-d$	$-d$	d
		y	d	d	$-d$	$-d$
		z	d	d	d	d
	$j=1$	x	x_0	$-x_0$	$-x_0$	x_0
		y	x_0	x_0	$-x_0$	$-x_0$
		z	z_0	z_0	z_0	z_0
Chlorine	2	x	z_0	$-z_0$	$-z_0$	z_0
		y	x_0	x_0	$-x_0$	$-x_0$
		z	x_0	x_0	x_0	x_0
	3	x	x_0	$-x_0$	$-x_0$	x_0
		y	z_0	z_0	$-z_0$	$-z_0$
		z	x_0	x_0	x_0	x_0

$x_0 = 0{\cdot}10$ Å $d = 0{\cdot}44$ Å $z_0 = 2{\cdot}14$ Å

The predominant part of the scattering comes from single-molecule disorder. Different model calculations demonstrate clearly that the molecules perform large-amplitude librational motions around their equilibrium position. A good description can be obtained when we assume that this motion is only limited by steric hindrance effects, occurring between a particular molecule and its eight nearest neighbours. Disorder effects caused by the different molecular and lattice site symmetry lead to very weak and unobservable diffuse intensities. Therefore the single-molecule part of the disorder in C_2Cl_6 should be comparable with molecular crystals built up from molecules with the symmetry $m3m$, in particular with SF_6, which has been investigated recently with simulation techniques (Dove & Pawley, 1984).

Highly modulated weak scattering - predominantly at small angles - reveals correlation effects in the orientation of neighbour molecules treated in the molecular-field approximation. An energetically favourable arrangement is obtained when the trigonal molecular axis of nearest-neighbour molecules order parallel to the cubic body diagonals. This leads to short-range one-dimensional order which results in the appearance of (111) planes of diffuse scattering. This is in qualitative agreement with experiment. Apparently no pronounced correlation effects occur along the {100} direction where the close contact of two chlorine atoms belonging to two different next-nearest-neighbour molecules is expected to cause strong steric hindrance (*cf.* Dove & Pawley, 1984). Related diffuse (100) planes or streaks, which would be present in the case of a two-dimensional order, are not observable.

The reported orientational short-range order is in agreement with the fully ordered orthorhombic low-temperature structure (Hohlwein, Nägele & Prandl, 1979), in which the trigonal molecular axes are lying in planes, slightly tilted but parallel to one another. At a smaller centre-of-mass separation the energetically favoured configuration changes to a perpendicular arrangement of the trigonal molecular axes. This configuration is realized in the low-temperature phase of ethane (C_2H_6; van Nes & Vos, 1978). In C_2Cl_6, however, the replusion of the relatively large chlorine atoms prevents the development of this structure even at low temperatures. A comparison of the low- and high-temperature phases in hexachloroethane suggests furthermore that the orientational ordering has a strong effect on the symmetry and the dimensions of the crystalline lattice. This causes a presumably correlated change in the centre-of-mass arrangement as well as the equilibrium orientational states. These effects are not considered in the present theory and lead to the observed first-order phase transition. The resulting change in the centre-of-mass structure prevents the development of the orientational order predicted in this theory.

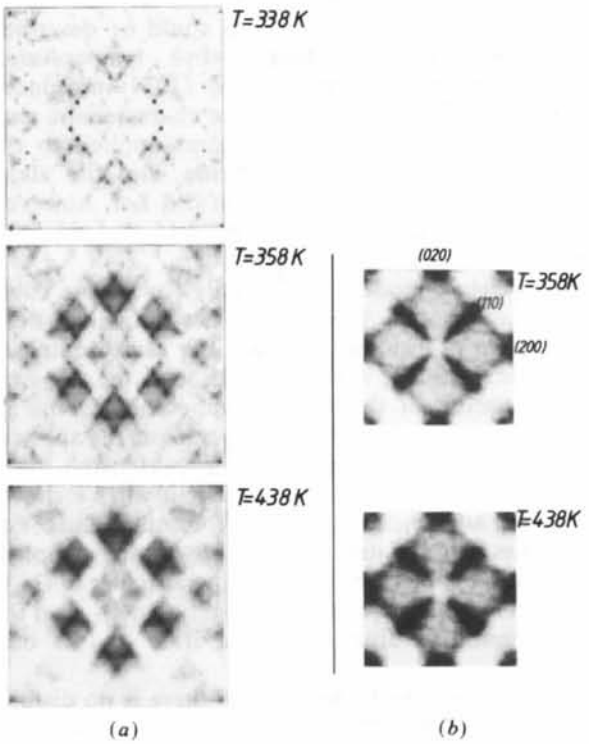

Fig. 7. (*a*) The calculated diffuse intensity due to orientational correlations [equations (1), (2)] for the scattering plane (110) shown in Fig. 2(*b*) at three different temperatures. (*b*) Detail section for the scattering plane (100) shown in Fig. 2(*a*). The linear densitogram is identical to the one used in Fig. 5.

References

BEE, M. (1985). *J. Chim. Phys. Phys. Chim. Biol.* **82**, 205–218.

DESCAMPS, M. & COULON, G. (1981). *J. Phys. C*, **14**, 2297–2304.

DOLLING, G., POWELL, B. M. & SEARS, V. F. (1979). *Mol. Phys.* **37**, 1859–1883.

DOVE, M. T. & PAWLEY, G. S. (1984). *J. Phys. C*, **17**, 6581–6599.

GERLACH, P., HOHLWEIN, D., PRANDL, W. & SCHULZ, F. W. (1981). *Acta Cryst.* A**37**, 904–908.

GERLACH, P., PRANDL, W. & LEFEBVRE, J. (1983). *Mol. Phys.* **49**, 991–999.

GERLACH, P., PRANDL, W. & VOGT, K. (1984). *Mol. Phys.* **52**, 383–397.

GUINIER, A. (1963). *X-ray Diffraction in Crystals, Imperfect Crystals and Amorphous Bodies.* San Francisco: Freeman.

HOHLWEIN, D., NÄGELE, W. & PRANDL, W. (1979). *Acta Cryst.* B**35**, 2975–2978.

KUBO, R. (1957). *J. Phys. Soc. Jpn*, **12**, 570–586.

MATSUBARA, T. (1949). *X-rays (Japan)*, **5**, 102–111.

MATSUBARA, T. (1950). *X-rays (Japan)*, **6**, 15–19.

NAGAI, K. (1982). *J. Phys. Soc. Jpn*, **51**, 4015–4020.

NAYA, S. (1974). *J. Phys. Soc. Jpn*, **37**, 340–347.

NES, G. J. H. VAN & VOS, A. (1978). *Acta Cryst.* B**34**, 1947–1956.

PRESS, W. (1981). *Single Particle Rotations in Molecular Crystals.* Berlin: Springer.

Acta Cryst. (1988). A**44**, 136-142

The Debye–Waller Factor for Polyatomic Solids. Relationships Between X-ray and Specific-Heat Debye Temperatures. The Debye–Einstein Model

BY R. D. HORNING

Honeywell Physical Sciences Center, 10701 *Lyndale Avenue South, Bloomington, MN* 55420, *USA*

AND J.-L. STAUDENMANN

Howard Hughes Medical Institute, E. E. Department-Columbia University, Brookhaven National Laboratory, NSLS-X4/Bldg 725, *Upton, NY* 11973, *USA*

(*Received* 8 *May* 1987; *accepted* 18 *September* 1987)

Abstract

The Debye-Waller factor for a polyatomic crystal is derived in the Debye approximation. If the crystal has a basis of p atoms per lattice point, it is shown that the specific-heat Debye temperature, Θ_D, and the X-ray Debye temperature, Θ_M, are related by $\Theta_D \simeq \Theta_M p^{1/2}$ in the classical limit. The Debye and Einstein theories are then combined to yield an expression for the Debye-Waller factor of a polyatomic solid. The acoustic phonon modes are described with a Debye approximation, and the optic modes with an Einstein model. For temperatures above the Debye temperature, the Debye and Einstein parts of the Debye-Waller factor have the same dependence on temperature and diffraction vector. Thus, the two parts cannot be distinguished.

I. Introduction

In general, the thermal vibration of the atoms in a crystal causes the intensities of Bragg reflections to decrease. The vibration magnitude of an atom in a unit cell primarily depends upon the temperature, its mass, and its surroundings: the way it is bonded to its neighbors (local symmetry). That is, each kind of atom in a unit cell has its own vibration amount which, in general, is anisotropic, and its effect on diffracted intensities is referred to as the temperature factor or as the Debye-Waller factor. In the case of isotropic vibrations, a Debye temperature Θ_M can be extracted from such factors. The physical interpretation of temperature factors is direct when discussions are restricted to diffraction measurements. However, the connection between thermal parameters and Debye temperatures extracted from specific-heat (Θ_D) or thermal-expansion measurements is difficult.

In 1912, Debye published the theory of specific heat in solids. Two years later, he succesfully quantified the decrease of X-ray intensities (Debye, 1914) where Θ_M, the characteristic Debye temperature, is introduced as the key parameter. Subsequently, Zener & Bilinsky (1936) showed that Θ_M is not exactly the same as the Debye temperature, Θ_D, of the specific-heat model. The difference is in the averaging between the velocities of the longitudinal and transverse phonons. Later, Barron, Leadbetter, Morrison & Salter (1966) stated that Θ_M should deviate from Θ_D by only a few percent. Expanding on Blackman's (1956) ideas, Barron *et al.* (1966) further pointed out that this approximation does not hold in all cases since real crystals do not strictly obey the Debye assumptions. Moreover, they demonstrated that more realistic frequency distributions could be described by temperature-dependent Debye temperatures, $\Theta_D(T)$ and $\Theta_M(T)$. Later, Reeber (1974) introduced a correspondence between lattice characteristic temperatures and Debye temperatures applied to the zinc-blende, the caesium chloride, and the alkali halide structures. These authors did not, however, show a relationship between Θ_D and Θ_M, which is one of the goals of this paper.

The Debye model is valid only for simple cubic monatomic solids. However, it has frequently been applied to polyatomic crystals. The same equations and nomenclature are used, although the physical interpretation of the Debye temperature is not as clear. It is the purpose of this paper to put the application to polyatomic crystals on a more rigorous basis. In contrast to the monatomic case, it will be shown that Θ_M and Θ_D differ widely for compounds. For purposes of illustration, the formalism will be applied to diatomic solids (see Table 1), in particular to GaAs and CdTe where the agreement between Θ_D and the corresponding value calculated from Θ_M is outstanding.

In the modified Debye theory, there is no distinction between the acoustic and the optic branches of the phonon dispersion curves. That is, all branches are equivalent. Integrations are done in an 'extended' Brillouin zone, which has a volume containing a number of wave vectors equal to the number of atoms in the crystal. A more realistic approach is outlined below, in which the Debye expression is used for the acoustic modes only and the optic modes are grouped

0108-7673/88/020136-07$03.00